

Gamma/hadron segregation for ground based imaging atmospheric Cherenkov telescope using the machine learning methods: Random Forest leads

Mradul Sharma¹ *, J. Nayak², M. K. Koul¹, S. Bose² and Abhas Mitra¹

¹ Astrophysical Sciences Division, Bhabha Atomic Research Centre, Mumbai, India;

² The Bayesian and Interdisciplinary Research Unit, Indian Statistical Institute, Kolkata , India

Received ; accepted

Abstract A detailed case study of γ -hadron segregation for a ground based atmospheric Cherenkov telescope is presented. We have evaluated and compared various supervised machine learning methods such as the Random Forest method, Artificial Neural Network, Linear Discriminant method, Naive Bayes Classifiers, Support Vector Machines as well as the conventional dynamic supercut method by simulating triggering events with the Monte Carlo method and applied the results to a Cherenkov telescope. It is demonstrated that the Random Forest method is the most sensitive machine learning method for γ -hadron segregation.

Key words: methods: statistical — telescopes

1 INTRODUCTION

Multidimensional datasets are very difficult to handle with conventional methods, which are generally linear in nature. Therefore, when multidimensional data are encountered, the efficiency of these methods reduces drastically as any interdependence among various parameters is beyond the realm of linear methods. In the case of ground based atmospheric Cherenkov systems, the typical characterization of a signal involves more than four attributes/parameters. Present day Cherenkov systems are operating in an energy regime where conventional methods are losing their edge on account of fading differences among the discriminating attributes/parameters between signal and background. Therefore, the ground based gamma ray astronomy community has started exploring various options including multivariate methods. These multivariate methods fall under the umbrella of machine learning methods. The simplicity and intrinsic ability of these methods to scrub out interdependence, if any, among various attributes/parameters has made the field of machine learning methods one of the fastest growing scientific disciplines. These methods employ

statistical tools to decipher hidden relationships, if any, among a few or a collection of attributes/parameters with comparatively little computing infrastructure.

Machine learning methods have been explored in the field of ground based gamma ray astronomy for quite some time. The earliest efforts were initiated by Bock et al. (2004). Later on, for γ -hadron segregation, the effectiveness of tree based multivariate classifiers was demonstrated by two operational ground based observatories, MAGIC (Albert & co-authors. 2008) and HESS (Ohm et al. 2009; Fiascon et al. 2010; Dubois et al. 2009). It should be noted that no machine learning method is sacrosanct as far as its superiority over other multivariate methods is concerned. Each dataset is unique and the classifier's performance is dependent on the dataset under investigation. Therefore, in order to assess the suitability of a classifier, each dataset needs to be probed independently. In this paper, we compare and evaluate various supervised machine learning methods to assess their suitability for γ -hadron segregation. A total of five machine learning methods, namely Random Forest (RF), Artificial Neural Network (ANN), Linear Discriminant Analysis (DISC), Naive Bayes (NB) Classifier and Support Vector Machine (SVM) with the Radial Basis Function (RBF) and polynomial kernel have been investigated. They are selected in a way to represent a type of machine learning stream. Among these five methods, the RF method represents a logic based algorithm. The ANN methods are perceptron based techniques. On the other hand, DISC and NB Classifier are statistical learning methods. Furthermore, SVM represents a rather new (1992) machine learning technique. The signal strength after classification by each machine learning method was compared with respect to the conventional dynamic supercut method and a conclusion is reached to select the best classification method.

The plan for the paper is as follows: In Section 2, a brief summary of ground based atmospheric Cherenkov telescopes and the underlying principle will be outlined. Section 3 involves the description of the database used to compare various machine learning methods. The subsequent section provides an overview of all the machine learning methods. The final two sections deal with a critical analysis of all the classifiers and the conclusion respectively.

2 GROUND BASED ATMOSPHERIC CHERENKOV SYSTEMS

Ground based gamma ray astronomy is a rather new discipline. The first successful detection of the TeV source Crab Nebula (Weekes et al. 1989) took place in 1989. With a brief lull in the field, the next detection took place in 1992 when the second TeV γ -ray source Markarian 421 (Punch et al. 1992) was detected and subsequently in 1996, Mrk501 (Quinn et al. 1996) was detected. Slowly a series of such extragalactic sources was discovered. With the advent of more sensitive systems, the catalog¹ of TeV γ -ray sources saw the addition of newer sources. The present day field of ground based gamma ray astronomy is flourishing with new detections of exotic sources. In fact, so far more than 150 galactic and extragalactic sources have been discovered.

The detection of cosmic γ -ray sources is based on the principle of the detection of Cherenkov photons produced by cosmic rays in the atmosphere. When cosmic rays enter the atmosphere, they interact with atmospheric nuclei by hadronic and electromagnetic interaction. Electrons and the cosmic γ -rays interact electromagnetically, i.e. they generate secondary particles by '*pair production*' and the '*bremsstrahlung*'

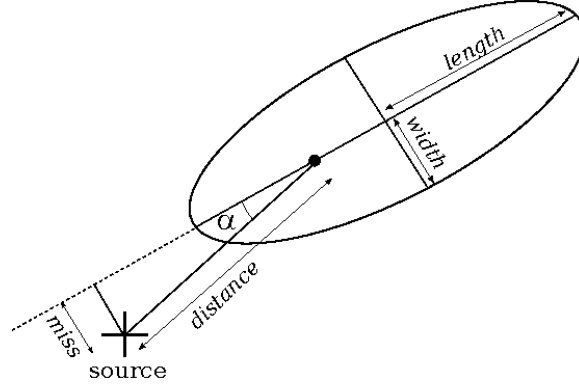


Fig. 1 Diagram of a few image parameters.

process. The hadronic cosmic rays, namely protons and ionized nuclei, interact via the hadronic interaction and also give rise to a number of secondary particles. Such generation of secondary particles in the atmosphere is called the *Extensive Air Shower*. The hadronic showers create π^0 particles that decay into γ -rays making it difficult to distinguish these hadronic showers from genuine showers initiated by γ -rays. The segregation of showers initiated by γ -rays is quite challenging because cosmic rays far outnumber the γ -rays by a huge margin.

2.1 The Imaging Atmospheric Cherenkov Technique

The secondary particles generated in extensive air showers move with relativistic speeds and generate Cherenkov radiation in the atmosphere. The technique of detecting the Cherenkov photon image is known as the Imaging Atmospheric Cherenkov Technique (IACT). If the shower is close enough to the telescope, the Cherenkov photons are reflected by the telescope's reflecting dish and get focused on the camera (an array of photomultiplier tubes in the focal plane of the detector). The geometrical projection of the shower onto a detector is called an *image*. The IACT is used to differentiate between γ and hadron initiated showers on the basis of the shape and orientation of the images. The image parameterization was introduced by *Hillas* and hence these parameters are known as Hillas parameters (hillas 1985). Image properties (analyzed offline) provide information about the nature, energy and incoming direction of the primary particle triggering a shower. A representative diagram of the Hillas parameter is shown in Figure 1.

3 DATABASE USED IN THIS STUDY

A database of Monte Carlo simulations was generated by using the CORSIKA air shower code (Heck et al. 1998) with the Cherenkov option. The simulations were carried out for the TACTIC telescope (Koul et al. 2011) located at the Mount Abu observatory, with an altitude of ~ 1300 m. The simulated showers were generated at zenith angles of 5° , 15° , 25° , 35° and 45° . The imaging camera with a total of 349 pixels was considered with the innermost 121 pixels being used for generating the trigger. The Cherenkov photons triggered the telescope after encountering the wavelength dependent photon absorption, reflection coeffi-

tubes. All the triggered events underwent the usual image cleaning procedures described in the literature (Konopelko et al. 1996) to eliminate background noise.

The simulated events triggering the telescope were selected according to the differential spectral index 2.6 and 2.7 for γ and protons respectively. The γ events were generated in the energy range from 1–20 TeV. The corresponding proton events were generated from 2–40 TeV. In order to have a robust and well contained image inside the camera, the prefiltering cuts of size (photoelectrons) ≥ 50 and a distance cut of $0.4^\circ \leq \text{distance} \leq 1.4^\circ$ were applied. This process yielded a total of 7938 events for both γ and protons.

3.1 Image Parameters for Classification

Various Hillas image parameters (hillas 1985) like length, width, distance, size (photoelectron) and zenith angle can be used in the process of γ -hadron segregation. However, the size parameter as well as the zenith angle parameter are not strictly separation parameters for γ -ray and hadronic showers. In particular, the zenith angle, for instance, by itself cannot be used to separate the events although different image parameters depend on it. The same is true with the size (photoelectron) parameter. A typical problem with these parameters is that in case the training samples for γ -ray and hadrons have a different distribution in these parameters, these parameters may be considered as separation parameters. This may lead to a rather risky situation, which is typically handled by preparing the training samples in such a way that their distributions on those parameters (typically size and zenith) are as close as possible. In this way, the uncertainty associated with using such parameters as separation parameters can be avoided. In this study, such complexities have been taken into account. In addition to these parameters, a derived parameter ‘dens,’ defined (Hengstebeck 2007) as

$$\text{dens} = \frac{\log_{10}(\text{size})}{\text{length} \times \text{width}} \quad (1)$$

was also used. A total of two sets of image parameters was considered. The idea was to investigate various classifiers as a function of the image attributes/parameters. In the first instance, only five image parameters: length, width, distance, size and frac2 (defined as the ratio of the sum of the two highest pixel signals to the sum of all the signals), were considered from the simulation database. In the second case, we considered a total of seven image parameters. Here, in addition to the above mentioned five parameters, two additional parameters, namely zenith angle and dens parameter, were also included. However, for classification purposes, the alpha parameter was not considered. The alpha is a very powerful parameter as it carries the signature of the progenitor (γ or proton). The alpha distribution is expected to be flat for cosmic ray protons, whereas it reflects a peaky behavior, for $\leq 18^\circ$ for γ -rays. In order to remove any bias of such a strong parameter, it was not considered for classification purposes. Moreover, this parameter plays a crucial role in the estimation of signal strength. If the alpha parameter is used in the classification, then the hadronic background cannot be evaluated.

4 DIFFERENT CLASSIFICATION METHODS

The problem of γ -hadron segregation is formulated as a two class problem: γ represents one class and the hadron is the second class. In the literature, a large variety of multivariate classification methods exists.

selected. The classification was carried out by using five different machine learning methods, namely RF, ANN, DISC, NB Classifier and SVM with the RBF and polynomial kernel. Except for the RF and the Dynamic Supercut methods, the other methods were applied from a commercially available package named STATISTICA². On the other hand, the RF method was studied by using the original RF code³.

4.1 Conventional Method: Dynamic Supercut

The spatial distribution of Cherenkov photons on the image plane of the camera is parameterized on the basis of the shape and size (light content) of each such image. The conventional parameterization leads to the estimation of the image parameters (hillas 1985). In this technique, various sequential cuts in the image parameters are applied so as to maximize the γ -ray like signal and reject the maximum number of background events. However, this scheme has a disadvantage because the width and length parameters grow with the primary energy. It is observed that the width and length of an image are well correlated with the logarithm of size; the size of the image provides an estimate of the primary energy. This method of scaling the width and length parameters with the size is known as the dynamic supercut method (Mohanty et al. 1998). By employing this method, the optimum number of cut parameters and their values are estimated by numerically maximizing the so called quality factor Q (Gaug 2001). The quality factor is defined as

$$Q = \frac{\epsilon_\gamma}{\sqrt{\epsilon_P}}, \quad (2)$$

where ϵ_γ and ϵ_P are γ and hadron acceptances respectively. The γ -acceptance is defined as the correctly classified γ events out of the total number of γ events and ϵ_P is the fraction of proton events which behave like γ events after the γ -hadron classification. The image parameters in Table 1 lead to the maximum quality factor.

Table 1 Dynamic Supercut Parameters

Parameter	Cut Value
Length (L)	$0.110^\circ \leq L \leq (0.235 + 0.0265 \ln(\text{size}))^\circ$
Width	$0.065^\circ \leq W \leq (0.085 + 0.0120 \ln(\text{size}))^\circ$
Distance (D)	$0.4^\circ \leq D \leq 1.4^\circ$
Size (S)	$S \geq 50 \text{ pe}$
Alpha (α)	$\leq 18^\circ$
Frac2	$\text{frac2} \geq 0.35$

4.2 Random Forest Method

The RF method is a flexible multivariate selection method. The algorithm for RF was developed by Leo Breiman and Adele Cutler⁴.

The RFs are a combination of tree predictors such that each tree depends on the values of a random vector sampled independently and with the same distribution for all trees in the forest (Breiman 2001). The

² STATISTICA <http://www.statsoftindia.com/>

³ http://www.stat.berkeley.edu/~breiman/RandomForests/cc_software.htm

classification trees, also known as “decision trees,” are machine learning prediction models constructed by recursively partitioning the data set. Each binary recursive partitioning splits the data sets into different branches. The tree construction starts from the root node (the entire dataset) and ends at a leaf. Every leaf node is assigned to a class. The RF method combines the concept of ‘bagging’ (Breiman 1996) and ‘Random Split Selection’ (?).

4.2.1 Bagging

The RF builds on the bagging (Breiman 1996) technique, where bagging stands for “Bootstrapping” and “Aggregating” techniques. The basic idea of bagging is to use bootstrap re-sampling to generate multiple versions of a predictor and combining them to make the classification. On the other hand, the bootstrapping is based on random sampling with replacement. It ensures that the probability of selecting an event in the sampling (with replacement) procedure is constantly $1/n$. Therefore, the probability of not selecting an event is equal to $(1-1/n)$. If the selection process is repeated n times, where n is very large, the probability of not selecting an event will be $\sim 1/3$. Therefore, only $2/3$ ($\sim 70\%$) of events are taken for each bootstrap sample.

4.2.2 Random split selection

In addition to bagging, RF also employs “Random Split Selection” (?). At each node of the decision tree, m variables are selected at random out of the M input vectors and the best split is selected out of these m . Typically about square root (M) = m number of predictors are selected. Two sources of randomness, namely random inputs and random features, make RFs accurate classifiers. In order to measure the classification power (separation ability) of a parameter and to optimize the cut value, the Gini index is used, which measures the inequality of two distributions. It is defined as the ratio between (a) the area spanned by the observed cumulative distribution and the hypothetical cumulative distribution for a non-discriminating variable (uniform distribution, 45° line), and (b) the area under this uniform distribution. It is a variable between zero and one; a low Gini coefficient indicates more equal distributions, while a high Gini coefficient shows an unequal distribution. Breiman (2001) estimated the error rate on out-of-bag data (i.e. oob data). Each tree is constructed on a different bootstrap sample. Since in each bootstrap training set about one third of the instances are left out (i.e. out-of-bag), we can estimate the test set classification error by applying each case that is left out of the construction of the t^{th} tree to the t^{th} tree. To be precise, the oob error estimate is the proportion of misclassification for the oob data.

In this study, the original RF code in Fortran⁵ was employed and a total of 100 trees was generated. The variable defined in the above code as $m_{\text{try}} = 2/3$ was taken. Very similar results were obtained in each case. The resultant output of this code was compared with the implementation of RF in the statistical package R⁶. It is worth mentioning here that the Fortran code encounters some memory issues when the number of training/test events crosses a certain threshold. However, this limitation was not encountered in the RF implementation in R.

⁵ <http://www.stat.berkeley.edu/~breiman/RandomForests>

4.3 Artificial Neural Network

The ANN consists of many inputs (Gershenson 2003) which are multiplied by weights (strength of the respective signals), and then computed by a mathematical function that determines the activation of the neuron. Another function computes the output of the artificial neuron. The specific output demanded by the user can be obtained by adjusting the weights of an artificial neuron. A multilayer perceptron (MLP) is perhaps the most popular network architecture in use today, due originally to Rumelhart and McClelland (Rumelhart et al. 1986) and discussed at length in most neural network textbooks (Bishop 1995). Each neuron performs a weighted sum of its inputs and passes it through the transfer function to produce the output.

In this work, we use an MLP network with five inputs, a minimum of three hidden units and a maximum of 11 hidden units. For classification tasks, the probabilistic output was generated and the misclassification rate was estimated.

4.4 Linear Discriminant Analysis

Linear Discriminant Analysis is also known as Discriminant Function Analysis (DFA). DFA combines aspects of multivariate analysis of variance with the ability to classify observations into known categories. It is a multivariate technique which is not only utilized in classification but also estimates how good the classification is. In this method, the discrimination functions like canonical correlations are constructed and each function is assessed for significance. The estimation of the significance of a set of discriminant functions is computationally identical to multivariate analysis of variances. After estimating the significance, one proceeds for classification. It generally turns out that first one or two functions play an important role while the rest can be neglected. Each discrimination function is orthogonal to the previous function.

In the present case, it is known that each class belongs to either γ or hadron; thus, the *a priori* probabilities of these classes are known. Accordingly, in this work, the prior probabilities are taken for classification.

4.5 Naive Bayes Classifier

Bayesian classifiers gained prominence in the early nineties and perform very well (Langley et al. 1992; Friedman et al. 1997). A Naive Bayes classifier is a generative classifier technique based on the concept of probability theory. The Bayes theorem plays a critical role in probabilistic learning and classification. The Bayes theorem states that

$$p(B/A) = \frac{p(A/B)p(B)}{p(A)}, \quad (3)$$

where $p(A)$ = Independent probability of A , $p(B)$ = Independent probability of B , $p(A/B)$ = Conditional probability of A given B , $p(B/A)$ = Conditional probability of B given A , i.e. the posterior probability.

In “Naive Bayes Classification,” the different variables/attributes/features are assumed to be strongly (naively) independent, i.e.,

$$p(\langle x_1, x_2, x_3 \dots x_n \rangle | y) = \prod_{i=1}^n \Pi(x_i | y). \quad (4)$$

Using the strong “independence assumption” and the prior probabilities, the most probable class for a given

gives

$$\arg \max_B p(B/A) = \arg \max_B p(A/B) p(B). \quad (5)$$

The training and evaluation from this method is very fast but the assumption of strong independence among parameters is a condition generally not satisfied in real world problems.

4.6 Support Vector Machine

The SVM was introduced by Boser et al. (1992). It is based on the concept of decision planes termed hyperplanes. These hyperplanes are constructed in multidimensional space for classification. The decision planes separate the classes. The linear decision plane is too limited in its application because of the heterogeneous nature of experimental data. In such a case, the linear decision plane lacks the ability to perform classification. Here nonlinear classifiers based on the kernel function play a vital role. The kernel function (mathematical function) maps the data into a higher dimensional hyperplane (feature space), where each coordinate corresponds to one feature of the data items. In this way, the data are transformed into a set of points in a Euclidean space, leading to the classification.

In the present work, the RBF and polynomial kernels are used. A polynomial of degree 3 with type 2 classification was employed. The parameters $\gamma = 0.2$ and $\nu = 0.5$ were considered. For the RBF, these parameters were 0.2 and 0.35 respectively.

5 COMPARISON OF CLASSIFICATION METHODS

The above listed methods were employed to classify the events into γ and hadron cases. A total of 7938 events of each type was considered as described in an earlier section. Around 70% of the events were used for training all the machine learning methods and the rest of the data was used as a test sample. The same training and test data were used by all the methods to have a one to one correspondence in the results. After training, the test sample was passed through the trained classifier and predictions of γ and hadron classes were made. Our aim is to identify the best classifier. The accuracy of the prediction rules can be evaluated by the Receiver Operator Characteristic (ROC) curves which are graphical techniques (Fawcett 2006) to compare the classifiers and visualize their performance. These curves are applied virtually in the field of decision making, like in signal detection theory (Egan 1975) and more recently in the medical field (Swets 1988).

5.1 Evaluation

We are considering a binary classification problem where the two cases are γ and hadrons. For a binary classification problem, a total of four outcomes are possible. Two outcomes are related to the correct classification for the two classes and two for incorrect classification. The True Positive (TP) class denotes the correct classification of class γ and True Negative (TN) class represents the correct classification of class hadron. The False Negative (FN) class reflects the class γ incorrectly classified as class hadron and False Positive (FP) class is the incorrect classification of class hadron as class γ .

The ROC plot is generated by using the above mentioned scenario for possible outcomes (TP, TN, FP,

(Fawcett 2006). The true positive rate is defined as

$$\text{TPR} = \frac{\text{TP}}{\text{TP} + \text{FN}} . \quad (6)$$

The hadrons classified as γ are represented by the False Positive Rate (FPR), defined as

$$\text{FPR} = \frac{\text{FP}}{\text{FP} + \text{TN}} . \quad (7)$$

TPR and FPR can be defined in terms of the fraction of correctly classified γ and hadrons. From Equations (6–7), it can be shown that

$$\text{TPR} = \epsilon_{\gamma} , \quad (8)$$

$$\text{FPR} = \epsilon_{\text{hadron}} . \quad (9)$$

Hence the TPR is the accepted γ fraction and the FPR is defined as the accepted hadron fraction. The best classifier is the one which provides the maximum TPR for the minimum FPR. It should be noted that we are not generating the ROC curves in the strict sense. The ROC curves lie between (0, 0) and (1, 1). In the present study, in order to better understand the results, the hadron rejection was plotted on a logarithmic axis. Therefore, the ROC plots in this study will differ from conventional ROC plots.

In order to find the best classifier, the decision boundary for prediction was varied. Each decision boundary generated one point in the γ -acceptance (TPR) and hadron acceptance (FPR) curves. These rates were plotted and the resultant plot is referred to as a decision-plot. The decision-plot was generated for each classifier. If the decision-plot skews towards the left side, it indicates greater accuracy, i.e. a higher ratio of true positive to false positive. In order to compare various classifiers, the decision plot is generated after the classification by all the methods. The top most plot in the decision-plot turns out to be the best classifier because for the same hadron acceptance, the upper plot gives the highest γ -acceptance.

The decision-plot is the qualifying metric to select the most suitable classification method. In addition to the decision-plot, the difference among various classifiers was also quantified by estimating the signal strength at a representative γ -acceptance value. The quantifying metric is designated as “signal strength” and defined as

$$\sigma = \frac{S}{\sqrt{(2B + S)}} , \quad (10)$$

where $S = \epsilon_{\gamma} N_S$ and $B = \epsilon_p N_B$ (Li & Ma 1983) are the signal and background events respectively. The signal strength was estimated by taking $N_B = 10\,000$ and $N_S = 500$ (Bock et al. 2004). Since the conventional dynamic supercut method estimated the γ -acceptance to be 57.4%, the hadron acceptance from each classifier was derived from the decision-plot at a γ -acceptance of 57.4%. The decision plot was generated for two sets of image parameters. As mentioned earlier, two sets were considered to evaluate the classification strength as a function of the number of image parameters. The decision-plots for these two cases are shown in Figure 2.

The comparison of decision-plot for RF methods for five and seven sets of image parameters shows that the RF method yields a better classification strength. This difference in the classification is, however, small and of the order of $\sim 10\%$ in the γ -ray acceptance for the given hadron acceptance range. This difference results because of the larger number of image parameters and guides us to choose more numbers

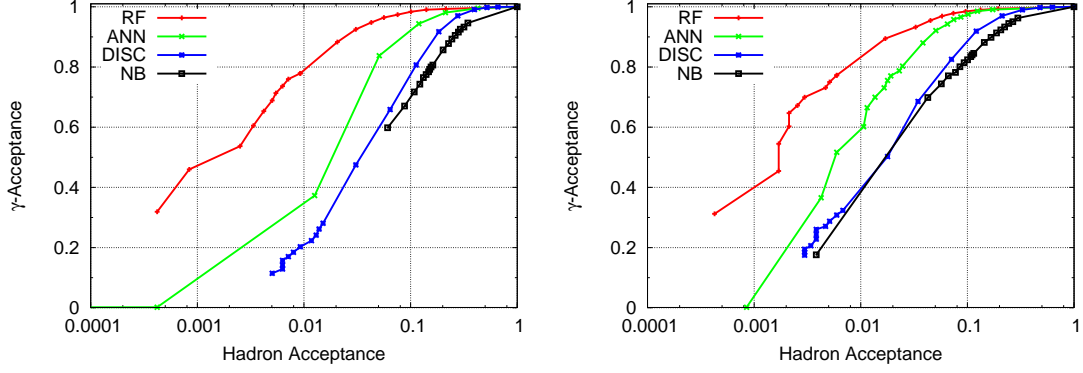


Fig. 2 Signal vs. background acceptance. The left panel is the classification result by using the five attributes/parameters. The right panel represents it for seven attributes/parameters.

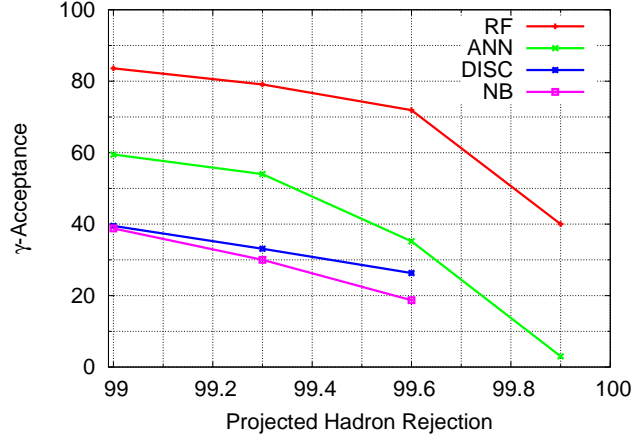


Fig. 3 γ -acceptance as a function of projected hadron rejection.

neural network method also reflects a tendency to prefer more numbers of image parameters for better classification. As per the decision-plot, the other two methods also indicate a positive effect on the classification strength with more numbers of image parameters. The decision plot provides an estimate of the possible γ -acceptance for a user chosen background (hadron) rejection. Any classifier yielding the maximum γ -acceptance for a given hadron acceptance decides the quality of the classifier. Figure 3 shows the γ -acceptance as a function of projected hadron-rejection for four representative projected hadron-rejection values, viz 99%, 99.3%, 99.6% and 99.9%.

For a hadron rejection of 99.9%, the RF method yields $\sim 40\%$ γ -acceptance. In comparison to this, any classifier coming closest to RF is ANN, which for the same hadron rejection secures a mere $\sim 3\%$ for γ -acceptance. The other two classifiers fail to go beyond 99.6% for projected hadron rejection. Furthermore, they yield a much smaller γ -acceptance compared to the above two classifiers, even at a projected hadron acceptance of 99.6%.

In addition to estimating the signal strength, the misclassification rate was also estimated by using a

Table 2 Misclassification Rate and Signal Strength with Five and Seven Image Parameters

Classification method	Misclassification Rate (%)	Signal Strength
	R_5/R_7	σ_5/σ_7
Random Forest	5.44/4.43	15.46 / 15.73
Automated Neural Network	7.40/5.82	9.8 / 13.30
Dynamic Supercut method	—	9.1 / 12.92
Linear Discriminant Analysis	12.11 / 10.08	8.10 / 10.37
Naive Bayes Classifiers	20.57 / 14.00	7.8 / 10.32
Support Vector Machine		
(i) with RBF kernel	9.18 / 16.08	na
(ii) with polynomial kernel	10.19 / 16.12	na

The positive effect of a greater number of parameters is better seen by a quantification of the misclassification rate as well as the signal strength. Table 2 shows that a higher number of attributes/parameters for training the classifier improves the signal strength while the misclassification rate goes down.

Such improvement in the misclassification rate as well as the signal strength is equally visible in all the classification methods. It should be noted that entries related to the SVM in Table 2 are absent. Only the misclassification rate is given. Many classification methods (ANN, DISC, NB) used in STATISTICA give the probabilistic output as well as the prediction probability, but there are instances where the prediction is a hard prediction, i.e. in terms of YES or NO output. In the case of SVM, the STATISTICA package yields hard predictions, thereby hindering the generation of a set of confusion matrices for different decision boundaries. Due to the lack of probabilistic output from SVM, it is difficult to estimate the signal strength. However, the misclassification rate from Table 2 for SVM with both the kernels (RBF and polynomial) suggests that for the given dataset, γ and hadron acceptances will remain lower compared to those of the RF and ANN methods. Based on this premise, it can be concluded that the SVM will not be able to match these two classifiers for our requirement.

Note that the strength of the ROC curves is generally exploited by comparing various classifiers and a suitable classifier is selected. The classifier is selected on the basis of its position in the ROC space. The top left most plot is considered to be the best classifier. However, this view of selecting the classifier on the basis of its position in the top left most part of the decision-plot is over simplistic. The Precision-Recall (PR) curves are more fundamental than the ROC plots. According to the theorem (Davis & Goadrich 2006), “For a fixed number of positive and negative examples, one curve dominates a second curve in the ROC space if and only if the first dominates the second in the PR space.” The precision is defined as

$$\text{Precision} = \frac{\text{TP}}{\text{TP} + \text{FP}}. \quad (11)$$

The precision essentially reflects the fraction of examples classified as positive which are truly positive, i.e. predicted positives (here class γ). The Recall is the TPR. In the PR space, the recall is plotted on the x -axis and the precision is plotted on the y -axis.

The classifier attaining the top position in the PR space and hence in the ROC space (as per the above

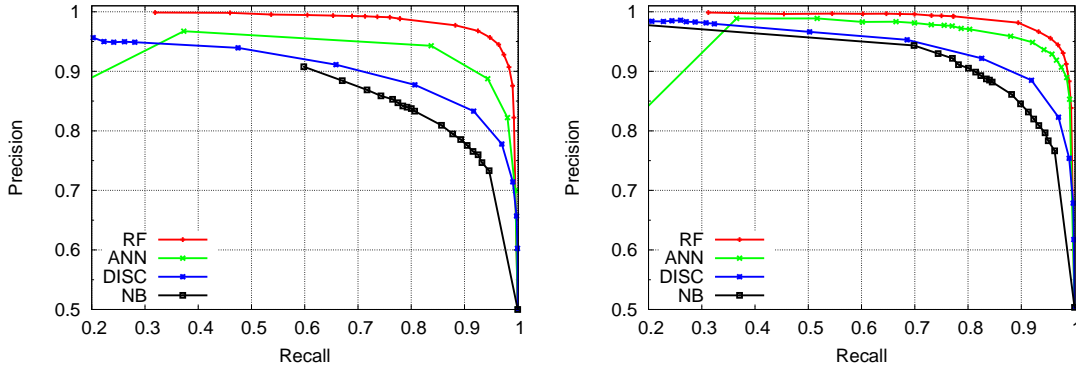


Fig. 4 PR curves. The left panel represents the PR curve for the five attributes/parameters. The right panel represents it for seven attributes/parameters.

best classifier, it is important to evaluate the classifier performance in the PR space. The PR plot is generated for both sets of image parameters and is shown in Figure 4.

The RF method retains the top most position in the ROC curve as well as in the PR space compared to the other classifiers. Therefore, on the basis of these two curves, it can be concluded that since the RF method dominates all the other classifiers, for the given dataset, it turns out to be the best classifier. It should be noted that the superiority of the PR curve over ROC plots is more pronounced when there is skewness in the class distribution of a dataset.

6 CONCLUSIONS

Five different machine learning methods were evaluated and compared to decide which of these methods is most suitable for γ -hadron segregation. Given the position of all the methods in the ROC space, the PR space and the misclassification rate for the given dataset, the trend reflects the superiority of RF and ANN compared to other methods, i.e. the DISC, NB Classifier and SVM. The signal strength was estimated by using a confusion matrix at a representative value for γ -acceptance of 0.574. This acceptance value was chosen because the conventional dynamic supercut method yields the same γ -acceptance. The dynamic supercut method yields a signal strength of $\sigma_{0.574} = 12.92$, whereas the signal strengths are 15.73 and 13.30 from the RF method and the ANN method respectively. It is clear that these two methods yield better results compared to the conventional dynamic supercut method. For the given dataset, the RF method gives an almost 20% improvement in the signal strength over the ANN method. A similar story is repeated in the estimation of the misclassification rate. It is of course difficult to make a generalized statement about the superiority of the RF method over any other method. Yet, the dominance of the RF method in the ROC plot as well as in the PR space indicates that for the given dataset, results are tilting in favor of the RF method. In addition to the above classifying metric, the RF method has an advantage in terms of computational time over the perceptron based methods, like ANN. As the number of perceptrons increases, it becomes very computationally expensive; an increase in the number of attributes/parameters adds to the computational expense. Also, unlike the ANN method, which acts as a black box, the RF method is quite

RF method takes care of parameters with little or no separation power, whereas ANN performance can be severely affected by the inclusion of such parameters.

In the next phase, a similar study will be carried out with a bigger dataset and the best method will be employed for γ -hadron segregation by taking experimental data. With the ever increasing data volume and the inclusion of larger numbers of attributes/parameters in the field of ground based γ -ray astronomy, the RF method, or rather the tree based method, is gaining all around popularity and soon it might become the preferred method of choice.

Acknowledgements MS thanks P. Savicky for making available the decision plot of the simulated MAGIC data. This helped in comparing the decision plot of their simulated data from our program.

Appendix A: VARIOUS MACHINE LEARNING METHODS

In addition to the five machine learning methods, various machine learning methods from the TMVA package (Hoecker et al. 2007) were tested and their resultant decision-plot is presented. Various machine learning methods are as follows: Boosting Decision Tree (BDT), BDT with gradient boost (BDTG), BDT with decorrelation (BDTD) + Adaptive Boost, TMlpANN (ROOT's own ANN), Fisher Boost (Linear discriminant with Boosting) and Probability Density Estimator Range-Search (PDESR). For all these methods, the default settings given by the TMVA developers were used. It is clear from the decision-plot (Fig. A.1) that the RF method outperforms all the other methods.

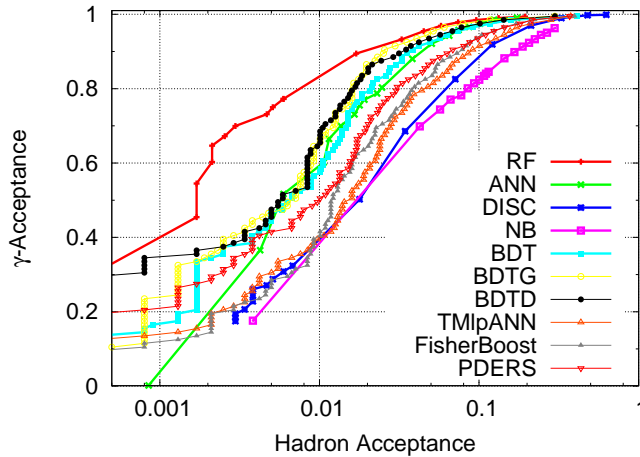


Fig. A.1 The decision-plot of various machine learning methods.

References

- Albert, J., & co-authors. 2008, Nuclear Instruments and Methods in Physics Research A, 588, 424
 Bishop, C. M. 1995, Neural Networks for Pattern Recognition (New York, NY, USA: Oxford University Press, Inc.)
 Bock, R. K., Chilingarian, A., Gaug, M., et al. 2004, Nuclear Instruments and Methods in Physics Research A, 516,

- Boser, B. E., Guyon, I. M., & Vapnik, V. N. 1992, in Proceedings of the fifth annual workshop on Computational learning theory, 144–152, COLT '92 (New York, NY, USA: ACM)
- Breiman, L. 1996, Machine Learning, 24, 41
- Breiman, L. 2001, Machine Learning, 45, 5
- Davis, J., & Goadrich, M. 2006, in Proceedings of the 23rd international conference on Machine learning, 233–240, ICML '06 (New York, NY, USA: ACM)
- Dubois, F., Lamanna, G., & Jacholkowska, A. 2009, Astroparticle Physics, 32, 73
- Egan, J. P. 1975, Signal detection theory and ROC analysis, Series in Cognition and Perception (New York, NY: Academic Press)
- Fawcett, T. 2006, Pattern Recogn. Lett., 27, 861
- Fiasson, A., Dubois, F., Lamanna, G., Masbou, J., & Rosier-Lees, S. 2010, Astroparticle Physics, 34, 25
- Friedman, N., Geiger, D., Goldszmidt, M., et al. 1997, in Machine Learning, 131–163
- Gaug, M. 2001, DESY-THESIS-2001-022
- Gershenson, C. 2003, CoRR, cs.NE/0308031
- Heck, D., Knapp, J., Capdevielle, J. N., Schatz, G., & Thouw, T. 1998, Forschungszentrum Karlsruhe Report FZKA, 6019, 1
- Hengstebeck, T. 2007, Measurement of the energy spectrum of the BL Lac object PG1553+113 with the MAGIC telescope in 2005 and 2006, Ph.D. thesis
- hillas, A. M. 1985, in International Cosmic Ray Conference, *International Cosmic Ray Conference*, vol. 3, edited by F. C. Jones, 445–448
- Hoecker, A., Speckmayer, P., Stelzer, J., et al. 2007, PoS, ACAT, 040
- Konopelko, A., Aharonian, F., Akhperjanian, A., et al. 1996, Astroparticle Physics, 4, 199
- Koul, M. K., Tickoo, A. K., Dhar, V. K., et al. 2011, Nuclear Instruments and Methods in Physics Research A, 646, 204
- Langley, P., Iba, W., & Thompson, K. 1992, in AAAI, 223–228
- Li, T.-P., & Ma, Y.-Q. 1983, ApJ, 272, 317
- Mohanty, G., Biller, S., Carter-Lewis, D. A., et al. 1998, Astroparticle Physics, 9, 15
- Ohm, S., van Eldik, C., & Egberts, K. 2009, Astroparticle Physics, 31, 383
- Punch, M., Akerlof, C. W., Cawley, M. F., et al. 1992, Nature, 358, 477
- Quinn, J., Akerlof, C. W., Biller, S., et al. 1996, ApJ, 456, L83
- Rumelhart, D. E., McClelland, J. L., & PDP Research Group, C., eds. 1986, Parallel distributed processing: explorations in the microstructure of cognition, vol. 1: foundations (Cambridge, MA, USA: MIT Press)
- Swets, J. A. 1988, Science, 240, 1285
- Weekes, T. C., Cawley, M. F., Fegan, D. J., et al. 1989, ApJ, 342, 379